Journal of Physics D:
Applied Physics

Sub-nanometer scale porosity emerging from SiOx plasma polymer films: characterization by positron annihilation spectroscopy

Journal of Physics D: Applied Physics

OPEN ACCESS

RECEIVED
7 November 2025

REVISED
8 December 2025

ACCEPTED FOR PUBLICATION
11 December 2025

PUBLISHED
30 December 2025

PAPER

Sub-nanometer scale porosity emerging from SiOx plasma polymer films: characterization by positron annihilation spectroscopy

Paula Navascués[1,*], Aurelio Garcia-Valenzuela[2], Maciej Oskar Liedke[3], Flaela Kalemi[1], Barbara Hanselmann[1], Maik Butterling[3,4], Eric Hirschmann[3], Andreas Wagner[3] and Dirk Hegemann[1,*]

[1] Plasma & Coating Group, Laboratory for Advanced Fibers, Empa, Swiss Federal Laboratories for Materials Science and Technology, Lerchenfeldstrasse 5, 9014 St. Gallen, Switzerland
[2] Institute of Ion Beam Physics and Materials Research, Helmholtz-Zentrum Dresden—Rossendorf, Bautzner Landstraße 400, 01328 Dresden, Germany
[3] Institute of Radiation Physics, Helmholtz-Zentrum Dresden—Rossendorf, Bautzner Landstraße 400, 01328 Dresden, Germany
[4] Reactor Institute Delft, Department of Radiation Science and Technology, Faculty of Applied Sciences, Delft University of Technology, Mekelweg 15, NL-2629 JB, Delft, The Netherlands
* Authors to whom any correspondence should be addressed.

E-mail: paula.denavascues@empa.ch and dirk.hegemann@empa.ch

Keywords: microporosity, plasma-enhanced chemical vapor deposition, hexametyldisiloxane, near-plasma chemistry, positron annihilation spectroscopy

Supplementary material for this article is available online

Abstract

The enhancement of microporosity in HMDSO-derived plasma polymer films through sequential cycles of plasma polymerization and etching has been demonstrated using positron spectroscopy techniques. These thin films exhibit a labyrinthine nanoporous architecture, characterized by an interconnected pore network with bottlenecks. The configuration of the plasma reactor significantly influences the final nanoporous structure, governed by the balance between ion-induced densification and chemical oxidation of residual hydrocarbons. By fine-tuning the plasma parameters and reactor design, small nanopores within the Si–O–Si cage structure are optimized to approximately 0.3 nm. These structural units are acting as interconnections of larger nanopores around 0.65 nm, functionalized with Si–OH groups along the pore walls. The high precision of positron annihilation spectroscopy enables clear differentiation between samples, with complementary insights provided by ellipsometry and Rutherford backscattering spectroscopy. Further optimization of the intrinsic microporosity was achieved through near-plasma chemical surface engineering, effectively mitigating ion-induced densification. Given the application potential of superhydrophilic SiOx-like thin films, the thermal stability of the nanoporous network was evaluated at moderate temperatures, revealing excellent structural integrity. These findings support the use of plasma polymer films fabricated via polymerization of hexamethyldisiloxane followed by etching as advanced membrane materials, where well-defined, defect-free microporous structures are essential.

1. Introduction

Advances in materials science during the past few decades have led the scientific community to redefine porosity in the nanoscale range. In particular, microporous insulating materials are attracting interest for many applications in different fields, from low-k dielectrics in microelectronics and semiconductor manufacturing [1] to advanced membranes with controlled permeability [2, 3] or biomedical platforms [4], among others. For all these applications, well-defined pore size and pore geometry as well as finely

tuned chemistry are required, besides proper adhesion on different substrates, high mechanical stability, or resistance to different environments such as, for example, oxidative ones or high temperatures.

Based on this scenario, nanotechnology is creating a new paradigm for low-k materials deposited as thin films. Low-pressure plasma technology allows precise control of the thickness at the nanoscale, allowing the fabrication of ultra-thin nanoporous coatings up to a few nanometers in a conformal manner [5]. Contrary to standard polymeric materials, plasma polymer films deposited at room temperature are highly crosslinked, amorphous materials [6]. Plasma polymerization, also known as plasma-enhanced chemical vapor deposition, induces intrinsic sub-nanometer scale porosity that is randomly defined during film growth, without the necessity for thermal curing needed as required for spin-on dielectrics [7]. The porous network is based on the deposition of film forming species together with the role of ion bombardment as well as surface reactions driven by the complex cocktail of plasma species, mostly radicals (depositing or etchants), photons, and electrons. For this reason, plasma polymer films are characterized by a labyrinthine nanoporous structure instead of well-directionally defined porous networks on a larger scale such as, for example, those deposited by glancing [8] and oblique [9] angle deposition techniques.

Although the intrinsic microporosity—pore size up to 2 nm—of plasma polymer films is well established, it has received relatively little attention, as the scientific community has instead focused on pore sizes in larger ranges. These plasma polymer films were interpreted as less porous materials with a closed porosity based on their high cross-linking degree. However, advanced applications have redirected attention to plasma polymers as promising nanomaterials during the past few years [10]. In this regard, the microporosity of plasma polymer films derived from siloxane monomers such as hexamethyldisiloxane (HMDSO) has been widely studied by different groups [11, 12]. During the past few years, our group has been working towards increasing the volumetric porosity of HMDSO-derived plasma polymer films by cycles of polymerization and etching of residual hydrocarbons [13–15], as well as by using them as functional coatings for different applications such as lubricant layers [14] or to control the delivery of radicals [16]. In particular, we have recently developed a novel plasma surface engineering approach, called near-plasma chemistry (NPC). This approach results in slightly enhanced volumetric porosity of films based on ellipsometry measurements. We relate this to a reduction of ion bombardment-driven damaging effects, avoiding densification, and promoting surface oxidation to end up in a robust SiOx-like chemistry [13].

Positron annihilation spectroscopy (PAS) is a powerful porosimetry technique to analyze polymeric materials on an atomic scale by probing the electron density distribution in the material [17]. In particular, for analyzing plasma polymer films, it stands out for the following reasons: (i) it allows the detection of pores below 1 nm size, thanks to the uniqueness of the probe as an antimatter particle (i.e. the antiparticle of the electron), (ii) it can determine *closed* porosity, ideal for the cross-linked structures studied in this work, (iii) it enables depth profiling at the nanometer scale, allowing differentiation between growth regimes, inhomogeneities, and damage occurring during film growth, and (iv) it is a non-destructive technique, allowing to measure the same sample under different conditions indicating whether porosity gets affected.

When positrons are injected into a material, they interact with electrons and annihilate, producing electromagnetic radiation that can be detected. While for conductive material positrons directly annihilate with the free electrons from the material, for insulators the scenario becomes more complex. In this regard, for porous polymeric materials such as the studied plasma polymer films, the key to study porosity is ortho-positronium. When positrons are injected into a material and approach a free volume unit, for example, a pore wall, they can bind electrons into a hydrogen-like state known as positronium (Ps). Therefore, the Ps is formed on the void wall by a positron picking an electron and escaping from the solid into a void or free space [18]. Depending on the orientation of electron and positron spins in the bound state, Ps decays in two photons (para-Ps) or three photons (ortho-Ps). While para-Ps quickly self-annihilate (lifetime of 0.125 ns), ortho-Ps live longer and therefore could be detected (lifetime of 142 ns in vacuum) or even further annihilate. Indeed, in porous materials, ortho-Ps interacts with surrounding electrons, the so-called pick-off annihilation, turning them into a 2γ decay, which is what is measured by PAS techniques and allows us to determine the average pore size [19, 20]. For this reason, the annihilation of ortho-Ps is strongly affected by the pore size and the surrounding chemistry [17]. In insulator materials, Ps preferentially locate in electron-deficient defects such as micro and mesopores. For HMDSO-derived plasma polymer films, pore walls are functionalized by dangling silanol (Si–OH) groups [14]. Electrons from these immobilized reactive groups in the plasma polymer network can easily interact with ortho-Ps.

Strong research by PAS groups over several decades has resulted in successful models to determine pore size distributions in the micropore range ($\leqslant$ 2 nm) for polymeric materials based on ortho-Ps interactions with voids/pores [17, 19, 20]. Within this study, it is our goal to discuss this powerful porosimetry technique along with other characterization methods based on different principles. Together with the matter-antimatter nature of PAS, we carried out a systematic study combining Rutherford backscattering spectroscopy (RBS), a matter-matter interaction method able to determine the density of elements in the coating, as well as estimating the refractive index of the material, in this second case, based on light-matter interaction principles by ellipsometry. It is important to mention that PAS cannot give a direct value for porosity, understood as volumetric porosity, rather indicating *open volume* or *void volume*. This is because of the important contribution of the annihilation in small defects as well as the contribution of para-Ps. For this reason, RBS and ellipsometry are used as complementary techniques to generally estimate volumetric porosity. Following the recent paper of Franke *et al* for HMDSO-derived plasma polymer films deposited on PET substrates [11], as well as previous studies from our group [13, 14] and others [12, 21], we use the terms *nanoporosity* and *microporosity* interchangeably to discuss the representative picture of our plasma polymer films, with the latter interpreted according to proper IUPAC classification (i.e. pore sizes below 2 nm define micropores).

This study thereby presents a systematic characterization of sub-nanometer porosity in plasma polymer films fabricated by cycles of polymerization and etching of the organosilicon deposit. To study the influence of ion bombardment on porosity, different films have been fabricated in symmetric and asymmetric plasma reactor configurations, as well as applying a novel NPC approach, thus varying plasma-surface interactions. A SiO_2-like barrier coating, typically used to hinder oxygen permeation and water transport, is used as a reference dense coating. In agreement with other studies, our porous plasma polymer films are characterized by small nanopores of around 0.3 nm pore size, interpreted as intrinsic pores in the Si–O network, as well as nanopores with pore size in the 0.5–0.7 nm range, representing the Si–OH functionalized pore walls. A minor contribution in the 0.7–2 nm range is detected, representing small defects, with no pores or defects detected larger than 2 nm, revealing a very well-defined pore size distribution. Based on the superhydrophilic nature of the coatings, heating the material in vacuum up to 230 °C allows to discard the water contribution, revealing a stable porous network with only a minor contraction of the coating observed after annealing, relevant for different applications.

2. Materials and methods

2.1. Plasma polymer film fabrication

The samples consisted of thin films fabricated by low-pressure plasma technology at room temperature. Two different plasma reactors were used, both capacitively-coupled (CCP) RF-driven (13.56 MHz) plasma reactors with symmetric and asymmetric configurations (see figure 1). The symmetric configuration contains two electrodes of 30 cm separated by 5 cm, and samples were located on the bottom driven electrode as shown in figure 1(a). The gas lines are distributed to ensure a homogeneous deposition rate through the full electrode area. On the other hand, the asymmetrical configuration comprises a rectangular electrode (21x70 cm^2) located at 9 cm distance to the (grounded) chamber wall. For this asymmetric configuration, samples were placed at the wall, as shown in figure 1(b). To further study the influence of ion bombardment on the microporosity of plasma polymer films, samples were fabricated by direct plasma exposure (DPE) or via near-plasma chemical surface engineering NPC. The latter consists of introducing a polymeric mesh in the plasma sheath, between the substrate and the bulk plasma, significantly reducing ion bombardment to the samples [13, 15]. The mesh is made of polyamide 6.6 (fibers 40 μm thick and separated by 240 μm), defining an open area of 78%. It was located 2.1 or 4 mm above the samples for the symmetric and asymmetric configurations, respectively, to ensure it stays in the plasma sheath [13].

The microporous thin films were fabricated combining cycles of plasma polymerization and etching, an experimental procedure previously reported by our group to obtain SiOx-like nanoporous films [14]. The deposition consisted of polymerizing the monomer HMDSO mixed with Ar and O_2 with a 1:2 Ar:O_2 ratio, keeping the same Ar/O_2 mixture for the subsequent etching steps. Plasma operating parameters were selected for optimized microporosity conditions based on previous research [13, 14]. For the symmetric configuration, for deposition, they were: 2 sccm of HMDSO, 10 sccm of Ar, 20 sccm O_2; applied pulsed power of 30 W, pressure of 20 Pa, deposition time of 44 s; etching time of 5 min for an applied continuous power of 20 W and pressure of 7 Pa. For the asymmetric configuration, the conditions were: 5 sccm HMDSO, 20 sccm Ar, 40 sccm O_2; applied power of 100 W, pressure of 7 Pa, deposition time of 3.5 min and etching time of 5 min. The number of cycles was adjusted for each process to end up with a similar coating thickness, with around 15 nm deposited per cycle [13, 14]. Immediately

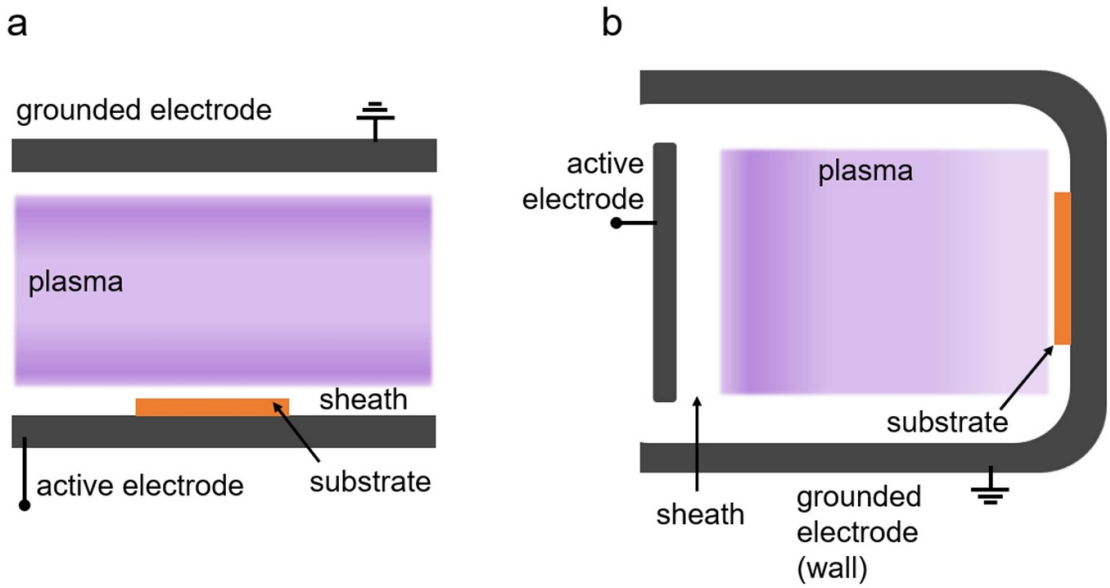

Figure 1. Scheme of RF CCP plasma reactor (a) symmetric and (b) asymmetric configurations.

before deposition all substrates were plasma cleaned with Ar/O_2 for 2 min. A dense SiO_2-like coating was fabricated in the asymmetric configuration placed at the active electrode, applying conditions to achieve a barrier coating, i.e. to hinder O_2 permeation and water transport [22–24]. Specifically, the conditions were 3 sccm HMDSO and 60 sccm O_2; applied power of 300 W, pressure of 4 Pa, deposition time of 20 min.

Samples have thicknesses in the range of 177 ± 56 nm, as measured by profilometry (Bruker Dektak XT), and a SiOx-like chemistry, with pore walls functionalized with—OH groups and containing residual hydrocarbons (-CHx groups) [13, 14]. The plasma polymer films were deposited on p-doped silicon wafers and on graphite foils, depending on the characterization technique.

2.2. PAS

Two different characterization techniques based on positrons were applied to study the microporosity of plasma polymer thin films at the Helmholtz–Zentrum Dresden–Rossendorf (HZDR) in Dresden, Germany. They were variable energy positron annihilation lifetime spectroscopy (VEPALS) and Doppler broadening variable DB-VEPAS, explained below. PAS methods are based on the interactions of a positron, implanted into a material at a defined depth (the so-called slow positron beam) and electrons of that material. When implanted into a solid, positrons lose their kinetic energy due to thermalization and after short diffusion annihilation usually emitting two anti-collinear 511 keV gamma photons once they meet electrons. This radiation is detected, providing structural information of the material at the nanoscale [17]. Coatings deposited on silicon wafers were used for the characterization.

2.2.1. VEPALS

VEPALS measurements were conducted at the Mono-energetic Positron Source beamline at HZDR [25]. Positron implantation energies (E_p) were varied between 1 and 11 keV with 1 keV step. A $CeBr_3$ scintillator detector coupled to a Hamamatsu R13089-100 photomultiplier tube was utilized for gamma photon detection. The signals were processed by the SPDevices ADQ14DC-2X digitizer (14-bit vertical resolution and 2GS/s horizontal resolution) [26]. The overall time resolution of the measurement system was around 0.25 ns and all spectra contained at least 10^7 counts. Obtained lifetime spectra are described based on the counterparts of different defect types contributing to the positron trapping, components with individual lifetimes τ_i and intensities I_i [27]. The instrument resolution function is a sum of two Gaussian functions with distinct intensities and relative shifts both depending on the positron implantation energy, E_p. It was determined by the measurement and analysis of a reference sample, i.e. amorphous yttria-stabilized zirconia, which exhibited a single well-known lifetime component. The background was negligible, hence fixed to zero.

Table 1. PAS lifetime components and correlation for microporous SiOx-like plasma polymer films.

Lifetime component	τ_B	τ_1	τ_2	τ_3	τ_4	τ_5
Interpretation	Annihilation in the matrix	Para-Ps and small defects	Small nanopores	Nanopores	Micropores	Mesopores
Approximate pore size (nm)[a]	—	—	∼ 0.3	0.45–0.70	0.70–2	>2
Chemistry	Bulk material	Small defects	Intrinsic pores Si–O network	Pore wall (–OH groups)	Larger pores and defect	—
Contribution	Minor	Minor	Major	Major	Minor	Not detected

[a] Pore size estimation based on the Tau–Eldrup model [19, 20], assuming spherical voids, also supported by the work of the Michigan positron group [17] for polymeric materials with pore size below 2 nm.

The positron annihilation lifetime has a characteristic value for elemental materials and defects. All the spectra were deconvoluted using a non-linear least-squares fitting method employed within the fitting software package PALSfit [28] into discrete lifetime components (τ_i) with defined intensity (I_i). These components directly evidence a combination of delocalized annihilation (bulk annihilation, τ_B), para-positronium (para-Ps) and localized annihilation in point defects (τ_1), annihilation at vacancy agglomerations and smallest micropores (τ_2), as well as larger micropore populations (τ_3 and τ_4). For the studied microporous thin films, components τ_2 and τ_3 are the most relevant ones, with more than 80% of the signal contributions. We will refer to them as the smallest nanopores (τ_2, pore size in the 0.3–0.45 nm range) and nanopores (τ_3, pore size in the 0.4–0.7 nm range). The less relevant component τ_4 corresponds to micropores in the 0.7–2 nm range, while a fifth component related to larger pore size (i.e. mesopores, higher than 2 nm) has not been detected for the studied samples. Table 1 summarizes the different lifetimes and their interpretation according to SiOx-like plasma polymer films as well as the related approximate pore size range. This interpretation is based on our results discussed in the next sections as well as the work of other authors with similar plasma polymers [11, 12].

The corresponding relative intensity (I_i) for each lifetime component τ_i primarily reflects the concentration of each defect type (size) if the size of the compared defects is in a similar range to that in the studied case. In general, the positron lifetime is directly proportional to the defect size, i.e. the larger the open volume is, the lower the probability and the longer it takes for positrons to be annihilated with electrons [27, 29]. The positron lifetime and its intensity have been probed as a function of positron implantation energy E_p or, in other words, implantation depth (thickness). The average positron lifetime τ_{av} is defined as $\tau_{av} = \sum_i \tau_i \cdot I_i$ and it has a high sensitivity to the defect type.

2.2.2. DB-VEPAS

DB-VEPAS measurements have been conducted at the apparatus for *in-situ* defect analysis [30] of the slow positron beamline (SPONSOR) [31]. For DB-VEPAS, positrons have been accelerated and implanted into samples with E_p in the 0.05–35 keV range. Since at the annihilation site thermalized positrons have a very small momentum compared to the electrons, a broadening of the 511 keV line is observed mostly due to the momentum of the electrons, which is measured with a high-purity Ge detector (energy resolution of 1.09 ± 0.01 keV at 511 keV). This broadening is characterized by two distinct parameters S (shape) and W (wing) defined as a fraction of the annihilation line in the middle (511 ± 0.70 keV) and outer regions (508.56 ± 0.30 keV and 513.44 ± 0.30 keV), respectively. The total area below the curve, which is utilized for the normalization of both parameters, is 511 ± 16.24 keV. The S-parameter is a fraction of positrons annihilated by low momentum valence electrons and represents vacancy type defects and their concentration. The S-parameter is sensitive to the signals originating from o-Ps annihilating by the pick-off process since two gamma photons are emitted, hence it provides insights regarding free volumes, too. The W-parameter approximates the overlap of positron wavefunctions with high momentum core electrons. While $S(E_p)$ plots provide depth dependent information, S–W plots visualize the atomic surroundings of the defect site as well as the defect size (type) [32].

Finally, DB-VEPALS can also provide information about the interconnectivity of the studied microporosity, discussing if voids are open or closed based on the evolution of the positronium in the material [33, 34]. Depending on the orientation of the electron and positron spins, Ps decays in two (2γ) or three photons (3γ). In condensed matter, the 3γ decay is suppressed due to the interaction with

the surrounding electrons (pick-off annihilation, turning into a 2γ decay), which indeed is what is measured by VEPALS [19, 20]. Hence, the ratio of the '$3\gamma/2\gamma$' is sensitive to the chemical environment of the Ps atom; while in perfect vacuum—closer to what could be defined as 'perfectly' interconnected pores—the ratio is about 3/1, in solids it drastically decreases. For the studied microporous plasma polymer films, the $3\gamma/2\gamma$ ratio will give a hint on the porous network interconnectivity, and, therefore, whether porosity is open, closed, or containing bottlenecks [7].

2.3. RBS

The samples were analyzed by RBS at the Van de Graaff accelerator of the HZDR. The incoming $4He^+$ beam had an energy of 1.7 MeV at an incident angle of 0° and a scattering angle of 170°. The analyzed area was about 1×1 mm^{-2}. All samples were mounted on the same sample holder in different sets, together with reference samples of Ni, C, Si, and Au for energy calibration of the detector. All samples were deposited on graphite foils (0.5 mm thick) to facilitate the determination of silicon and oxygen concentrations without any overlapping signals from the substrate.

The RBS spectra were fitted using the software SIMNRA version 7.01.1 [35]. For the fitting of the element composition, a stack model of the sample is built up from the surface to the substrate, which comprises all layers and the substrate. In some samples, more than one SiOx film was used, and hydrogen was also included to better determine the elemental composition of the films. The stoichiometry of the films, defined by the O to Si ratio, has been obtained from the areal density of each element ($\propto$ thickness of the film). Porosity, expressed as a percentage of void volume in the studied SiOx films, has been determined by comparing the density of the films (in at/cm^3) with that of the reference barrier coating. The density has been calculated by dividing the areal density (at/cm^2) by the film's thickness (cm), determined by profilometry.

2.4. Ellipsometry for refractive index estimation

The refractive index of the plasma polymer films was determined by ellipsometry with a Nanofilm EP4 device (Accurion) for samples deposited on Si wafers. The device operates with a fixed wavelength of 658 nm, varying the angle of incidence between 55° and 80°. Due to the transparency of the SiOx films in the visible range, the refractive index can be estimated by applying the Cauchy model and setting the extinction coefficient (k) to zero. By determining the refractive index of the material and using the volume averaging theory as an effective medium approximation [36]—note that the pore size is much smaller than the used wavelength—the porosity can be estimated. The SiO_2-like barrier coating is used as a dense reference with a measured refractive index of 1.503 [14].

3. Results and discussion

3.1. Enhancing microporosity combining plasma polymerization and etching

Depositing plasma polymer films from the HMDSO monomer provides a wide window of thin film properties that can be achieved based on plasma operating parameters. Surface chemistry can be adjusted by controlling applied power, pressure, and gas composition (e.g. adding reactive gases), allowing functional coatings with a precise control of their wettability [37]. Generally, to deposit microporous hydrophilic coatings, HMDSO is mixed with oxygen in the plasma, oxidizing most of the—CHx groups both in the gas phase and by surface reactions, ending up in the formation of nanoporous SiOx coatings with residual CH content [14]. We have carried out extensive research on the microporosity of these coatings by studying water diffusion, for example, by Neutron Reflectometry [38]. Moreover, the porosity of these coatings can be further increased by combining cycles of plasma polymerization and etching, ending up in superhydrophilic films allowing water to spread within seconds. Therefore, in each cycle around 15 nm SiOx(CH) layer is deposited, followed by Ar/O_2 plasma etching that removes the residual content of hydrocarbons, leaving a SiOx chemistry with enhanced nanoporosity [14]. Figure 2 shows VEPALS measurements for the evolution of the average positron lifetime with E_P for (gray curve) a conventional O_2/HMDSO-derived film (pp-SiOx), i.e. without intermittent etching and (blue curve) a SiOx film involving deposition and etching cycles (pp-etch-SiOx). As shown in the plot, the average lifetime clearly increases when performing cycles of plasma polymerization and etching, revealing a lower electron density and, therefore, larger voids and defects. As implantation energies give depth profiling information, both curves tend to overlap above 6 keV, when the substrate is clearly reached. Note that neither sharp decay nor full overlapping are achieved, mainly due to a broadening of the positron implantation profile with E_p, as at the higher energies a fraction of positrons still interact with the coating, showing a convoluted effect. We herein demonstrate the increase in microporosity by combining cycles of plasma polymerization and etching by VEPALS, in accordance with previous studies from our

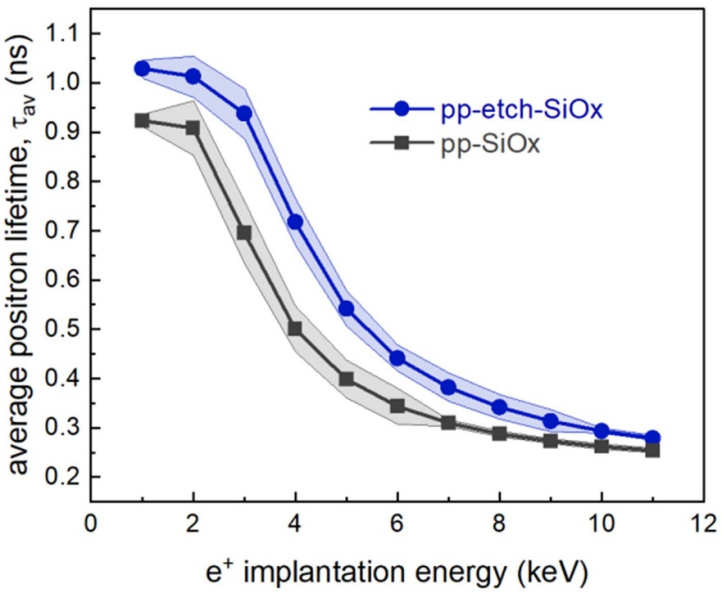

Figure 2. Average positron lifetime (τ_{av}) as a function of the positron implantation energy for SiOx films fabricated by only O_2/HMDSO plasma polymerization (pp-SiOx, gray plot) and by cycles of plasma polymerization and etching (pp-etch-SiOx, blue plot). Samples deposited in the symmetric reactor configuration at direct plasma exposure (cf figure 1(a)).

group using ellipsometry and other indirect measurements (e.g. water uptake) and molecular dynamic simulations [14], or by imaging the outermost surface by force microscopies [15].

Figure 3 shows the evolution of the relevant discrete lifetime components. The enhancement of the microporosity is clearly observed for pp-etch-SiOx coatings in the lifetime component τ_2 (cf figure 3(a)), associated with intrinsic nanopores around 0.3 nm size [12, 39], created in the Si–O network by removing residual hydrocarbons during the plasma etching step. This intrinsic porosity has also been defined by Franke *et al* as a *cluster of vacancies*, revealing a disordered—porous—system compared to a model SiO_2 lattice [11]. These authors observed a similar trend for τ_2 for SiOx plasma polymer films deposited on PET substrates when increasing the coating thickness, thus reducing the substrate influence on film growth. Indeed, polymer substrate influence on film growth is a relevant aspect. Hoppe *et al* for example, related τ_2 to localized annihilation at defects complexes within 20 nm SiOx layers deposited on PDMS substrates, while not discussing this component as porosity and focusing attention on τ_3 to τ_5 component, also detecting mesopores visible as large defects [21]. In our case, as shown in figure 3, the lifetime components τ_1, τ_3, and τ_4 do not significantly change for cycles of plasma polymerization and etching. The contribution of each lifetime component (i.e. intensity, I_i) remains constant for both coatings, as shown in S1, with the component τ_2 as the dominant one with a 60% contribution, indicating enhanced porosity.

The clear removal of hydrocarbons by consecutive cycles of plasma polymerization and etching is supported by RBS analysis, with an atomic contribution of 22% for the conventionally deposited sample, decreasing up to 5% when applying deposition/etching cycles—a clear tendency although RBS is not the ideal technique for very light elements. The decrease of hydrocarbons is counterbalanced by an embedding of oxygen into the coating, in agreement with our previous studies [13, 14], with an O/Si ratio of 2.07 and 2.13, for pp-SiOx and pp-etch-SiOx coatings, respectively. Clear differences in chemistry between these coatings are also observed in $S(E_p)$ and S–W plots shown in figure 4. Normally, the S-parameter scales with defect size and concentration, however, for heavily porous materials without large variation in pore sizes often reflect changes in metallicity and material chemistry, e.g. the abundance of CH-bonds. Clearly, higher values of the S-parameter (as inversed to the W-parameter) for the pp-SiOx sample—with SiOx(CH) chemistry—agree with the higher content of hydrocarbons and, therefore, a higher fraction of positrons annihilating with low momentum valence electrons, as shown in figure 4(a). On the contrary, the pp-etch-SiOx layer is characterized by lower values of the S-parameter. The plasma etching step also introduces additional cross-linking of the structure, both due to chemical oxidation and ion bombardment, which could result in lower S values. The S–W plot in figure 4(b) shows an increase in the W-parameter for the sample fabricated by cycles of polymerization and etching due to the higher oxygen content, while at low W values (and high S values) the plots overlap representing the

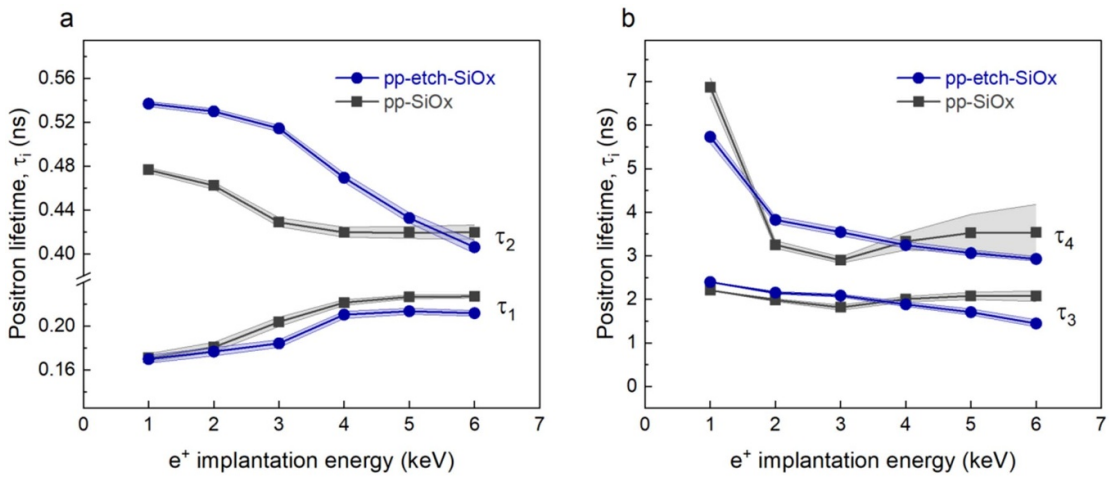

Figure 3. Discrete positron lifetime components (a: τ_1 and τ_2, b: τ_3 and τ_4) as a function of the positron implantation energy when using only O_2/HMDSO plasma polymerization (pp-SiOx, gray plot) and cycles of plasma polymerization and etching (pp-etch-SiOx, blue plot).

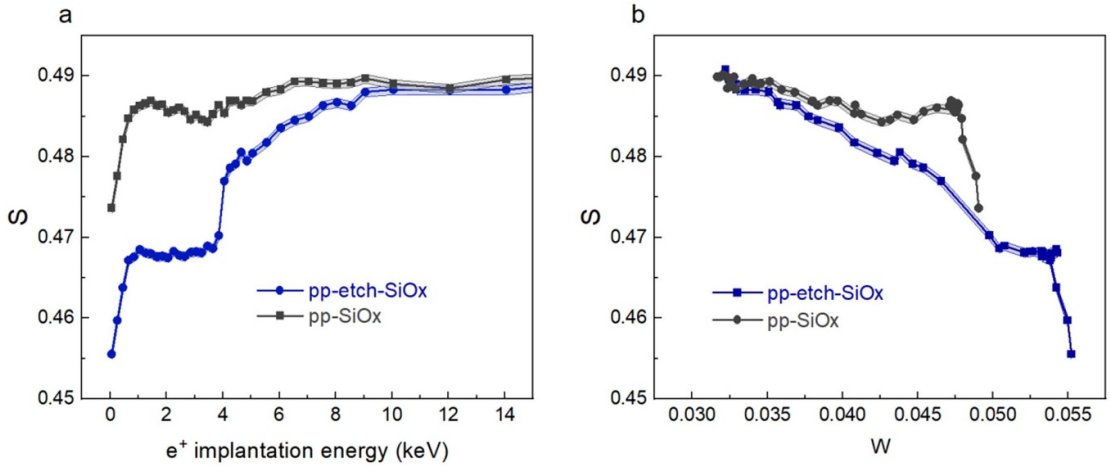

Figure 4. DB-VEPAS results for SiOx films using only O_2/HMDSO plasma polymerization (pp-SiOx, gray plot) and cycles of plasma polymerization and etching (pp-etch-SiOx, blue plot), showing the trend of the low electron momentum fraction (*S*-parameter) with (a) the positron implantation energy and with the (b) the high electron momentum fraction (*W*-parameter).

substrate. DB-VEPAS results in figure 4 agree with plots shown by other authors comparing SiOCH and SiOx plasma polymer film layers [40].

Variations in the plasma operating parameters when performing cycles of plasma polymerization and etching have an influence on the porosity of the coatings [13, 14]. As suggested by the results in figure 4, the plasma etching step might not only remove hydrocarbons but also increase the cross-linking degree of the coating, which might contribute to densification. Indeed, using the symmetric reactor configuration (as above), the power applied during the etching step has an influence on the total volumetric porosity, with higher values obtained for lower plasma etching powers (see S2). This fact inspired us to modify the experimental set-up to prevent possible negative effects caused by ion-induced densification.

3.2. Influence of ion bombardment on microporosity: controlling ion-induced densification

It is well accepted in the field of plasma-deposited coatings that energy transferred by ions during film growth can result in smaller pore sizes and densification [23, 41]. Asymmetric plasma CCP reactor configurations allow to locate samples at the grounded electrode (i.e. the reactor wall), significantly reducing the contribution of ion bombardment [13, 37]. Figure 5 shows nanopore sizes for SiOx coatings deposited with different plasma reactor configurations, at the grounded electrode of the asymmetric configuration, and at the active electrode of the symmetric configuration, as well as a reference SiO_2-like barrier coating deposited at the driven electrode in the asymmetric set-up. Note that the film fabricated in the symmetric configuration is the pp-etch-SiOx sample discussed before in section 3.1. The

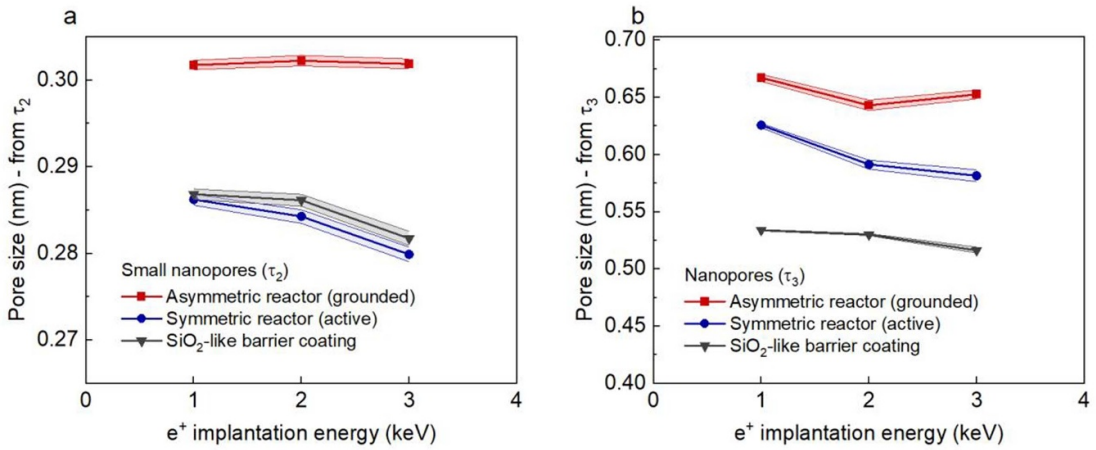

Figure 5. Pore sizes for (a) small nanopores (derived from τ_2) and (b) nanopores (derived from τ_3). Samples were fabricated at the active electrode of a symmetric reactor (c.f. figure 1(a), blue plot) and at the grounded electrode of an asymmetric reactor (cf figure 1(b), red plot), both using cycles of plasma polymerization and etching. A SiO_2-like barrier coating (gray plot) is used as a reference of a dense plasma polymer barrier layer.

discussed components are the major contributions to porosity, as indicated in table 1, with small nanopores around 0.3 nm (associated to τ_2, see figure 5(a)) and nanopores around 0.6 nm (associated to τ_3, see figure 5(b)). It can clearly be observed that deposition at the grounded electrode in the asymmetric configuration increases both ranges of pore sizes. For small nanopores, the sample deposited at the symmetric configuration overlaps with the barrier coating, probably related to SiOx densification effects due to ion bombardment, as shown in figure 5(a). However, both samples using cycles of plasma polymerization and etching yield larger nanopore sizes between 0.6 and 0.7 nm due to the incorporation of dangling Si–OH silanol groups at the pore wall, while for the barrier coating the nanopore size is defined between 0.50 and 0.55 nm. Similar tendencies have been reported by Hoppe *et al* comparing different input energies in an MW-driven plasma reactor [12]. Note that in figure 5 only 1–3 keV E_P data are plotted to restrict the analysis of pore sizes to the coating thickness. Full plots (1–11 keV E_P) of all discrete lifetime components τ_i and their intensities I_i can be found in S3, showing no significant differences between samples in intensities, again with the τ_2 component with a contribution of 60% and τ_3 around 25%. Micropores in the 0.7–2 nm range for microporous pp-etch-SiOx coatings have a minor contribution of approximately 5%.

As all discussed plasma polymer films in this section have a similar chemistry and structure, it is meaningful to systematically apply the Tau–Eldrup model [19, 20] to discuss pore size and intensity (i.e. concentration), assuming spherical voids. While the deduction of pore size in insulator materials is quite universal, their intensity is very sensitive to differences in chemistry and can be highly altered by tiny chemical differences [17]. Note that all coatings discussed in figure 5 are characterized by their overstoichiometry in oxygen, with Si/O ratios of 2.24 (asymmetric reactor, grounded electrode), 2.13 (symmetric reactor, active electrode), and 2.14 (barrier coating), all with carbon content below 10% as assessed by RBS. Similar chemistry of the materials allows a consistent discussion of $S(E_P)$ plots, as shown in figure 6(a), with a higher S-parameter for the more porous sample, i.e. the sample deposited in the asymmetric reactor at the grounded electrode. This result indicates reduced densification of the plasma polymer network due to less energy deposited by ions, ending up in higher microporosity. Similarly, higher values for the S-parameter at high W values are shown in the S–W plot for this sample (see figure 6(b)), in agreement with previous studies [40] and the higher oxygen content revealed by RBS and, therefore, a higher contribution of high momentum valence electrons.

3.3. Reducing ion-induced densification via near-plasma chemical surface engineering

Based on the verified densification effect by ion bombardment, the NPC approach (see section 2.1) was applied to potentially further increase microporosity in SiOx plasma polymer films. In a previous study [13], we demonstrated that the NPC approach, which limits ion bombardment by the introduction of a mesh between the plasma and the sample, allows obtaining well-defined Si–O–Si cage structures based on a more effective etching of residual hydrocarbons. These results were accompanied by an increase in porous volume up to 23% according to ellipsometry measurements—a remarkable feature considering plasma treatment close to room temperature [42]. VEPALS characterization allows us to confirm

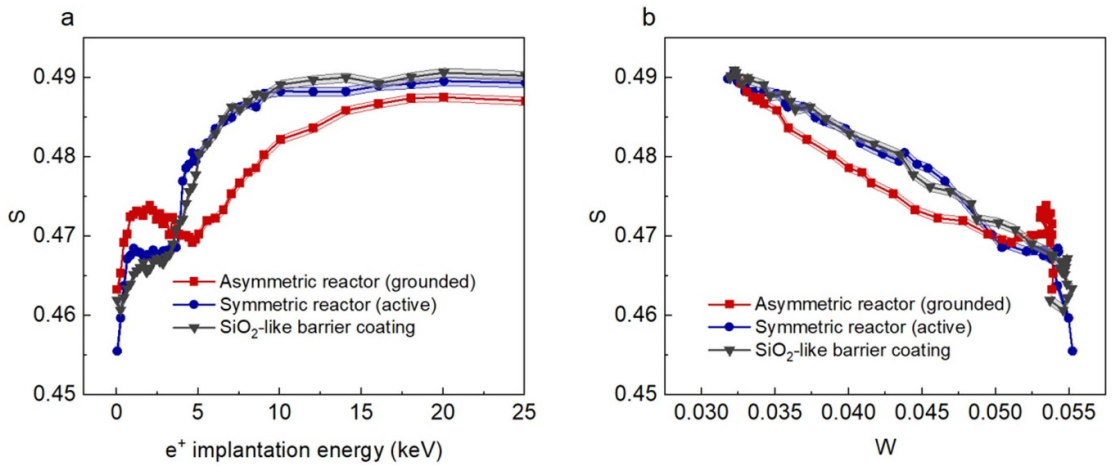

Figure 6. DB-VEPAS results for samples fabricated at the grounded electrode of the symmetric plasma reactor configuration (blue plot), at the grounded electrode of the asymmetric reactor (red plot), and a SiO_2-like barrier coating (gray plot). Sample deposition conditions as in figure 5. Low electron momentum fraction (*S*-parameter) is plotted with respect to (a) the positron implantation energy and (b) the high electron momentum fraction (*W*-parameter).

that this increase in porous volume is related to pore size distribution. Figure 7 shows nanopore sizes for samples fabricated at standard conditions DPE and applying NPC for depositing at the active electrode in the symmetric configuration (figures 7(a) and (b)) and at the grounded electrode in the asymmetric plasma reactor (figures 7(c) and (d)). The scale has been fixed for the two pore types to facilitate comparison. For the symmetric configuration, it can clearly be observed in figure 7(a) that the NPC approach increases the pore size of small nanopores (τ_2), revealing a more open Si–O–Si cage structure, as suggested in our previous work [13]. However, no differences are observed for larger nanopores (τ_3) in figure 7(b), which indicate that the distribution of silanol groups might be similar. For the asymmetric configuration, pore sizes for nanoporous components overlap for DPE and NPC samples (figures 7(c) and (d)). Apparently, the small nanopores defined in the Si–O–Si structure cannot reach higher values than 0.3 nm, and might act as interconnections between larger nanopores functionalized with silanol groups. These larger nanopores reach the highest values obtained by depositing them at the grounded electrode, optimized for around 0.65 nm size, as observed in figure 7(d).

The complete set of data for lifetime components τ_i and intensities I_i can be found in S4 for both plasma reactor configurations. In terms of pore intensities, in the first view, there are no significant differences between the different plasma coatings discussed in figure 7. However, it is important to note that VEPALS is a technique with very high sensitivity, able to detect minor but relevant differences in pore size and their intensity when discussing samples with similar chemistry and structure as in the present case. Although VEPALS cannot give a direct value for porosity, the *void volume*—understood as 'free' volume—can be determined based on each pore size and intensity [12, 21]. Assuming spherical pores, this can be calculated by the sum of multiplying each void size per the corresponding intensity; in our case, pore sizes resulting from lifetime components τ_2, τ_3, τ_4 and their corresponding intensities (I_2, I_3, I_4) (see equation (1)):

$$\text{Void volume}\,(\%) = p_2 I_2 + p_3 I_3 + p_4 I_4\,. \tag{1}$$

The concept of *void volume* can be related to the material porosity, although it is not equivalent [12, 21], as the contribution of annihilation in other small defects as well as of para-Ps cannot be discarded. Figure 8 shows void volume values based on equation (1), porosity estimations based on ellipsometry and on RBS characterization. While for ellipsometry the porosity is determined from the refractive index (see section 2.4), for RBS porosity it is calculated by comparison of the density of the coatings—determined from the areal density in at/cm^2—with respect to the reference barrier coating density. The three different techniques show a similar tendency for all samples. Ellipsometry provides the lowest values (between 13% and 23%), which can be related to residual carbon content, giving slightly higher refractive index values and, therefore, lower porosities. This is followed by RBS estimations (between 16% and 26%), and VEPALS void volume values (between 28% and 37%). Higher values are obtained when applying NPC (i.e. NPC samples) with respect to samples directly exposed to the plasma. Samples

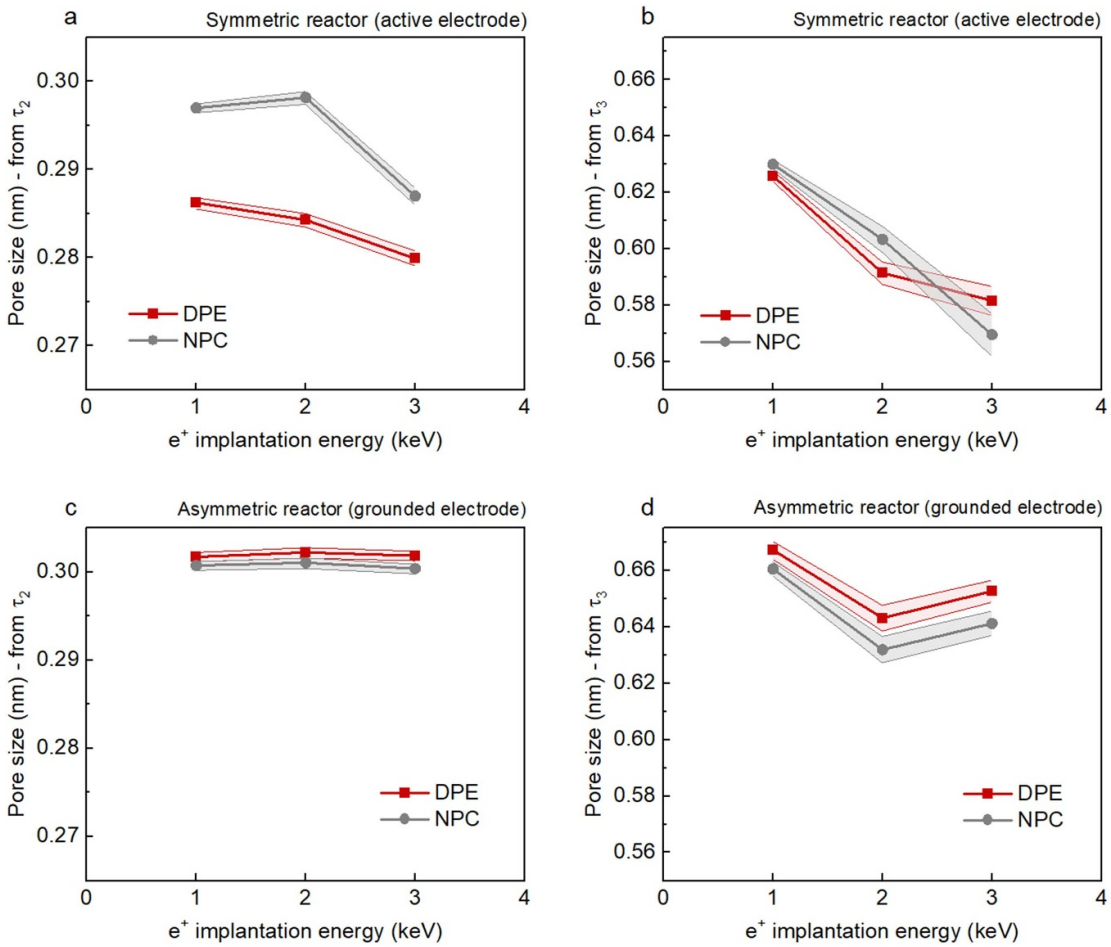

Figure 7. Pore size for (a), (c) small nanopores (derived from τ_2) and (b), (d) nanopores (derived from τ_3). Samples were fabricated at the active electrode of the symmetric plasma reactor (a), (b), and at the grounded electrode of the asymmetric reactor (c), (d), directly exposed to the plasma (DPE, red plots) and via near-plasma chemistry (NPC, light gray plots).

deposited at the grounded electrode in the asymmetric configuration present the highest porosity/-void volume values, in agreement with what has been discussed in previous sections. In particular, the NPC sample deposited at the asymmetric configuration is characterized by a porosity of 23% and 26% according to ellipsometry and RBS, respectively, while the void volume based on VEPALS achieves 36.8%.

The results shown in figure 8 differ in a reasonable way due to the drastically different underlying principles of the techniques: light-matter, matter-matter, and antimatter-matter interactions for ellipsometry, RBS, and VEPALS, respectively. While ellipsometry and RBS both determine open volume—based on the effective medium approach in the former and on the elemental density in the latter—VEPALS is a much more sensitive technique to additional contributions. While the contribution of para-Ps may be hidden in τ_1, hence does not directly affect void volume calculation (equation (1)), it rather offsets a baseline for it, as the ratio between para-Ps and ortho-Ps is defined as 1:3. Furthermore, we note that the ellipsometry characterization was performed using a standard device, not via ellipsometric porosimetry, which might provide additional insights [43]. The broad overview provided by the results in figure 8 is, in our opinion, the best way to discuss the examined microporous, highly cross-linked plasma polymer films, with porosity interpreted as total free volume or voids rather than directional channels. In the studied plasma polymer films, porosity is not directionally defined, but instead disordered and labyrinthine, unlike nanomaterials based on columnar film growth [44] or highly precise deposition techniques at the nanometer scale such as atomic layer deposition [45].

Table 2 summarizes the chemical characterization of the examined plasma coatings, with elemental composition (C, Si, O), density of Si and O atoms in the material, and their O/Si ratio. RBS spectra and fittings can be found in S5. Applying the NPC approach improves the etching of hydrocarbons, with a very low remaining contribution of C detected for these samples compared to coatings directly exposed to the plasma. This result agrees with recent findings of our group using FTIR [13] and time-of-flight

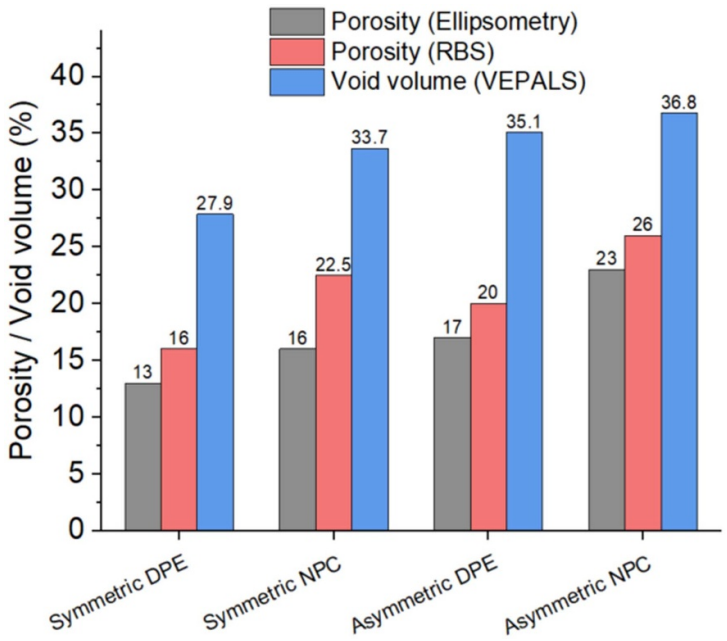

Figure 8. Porosity values based on ellipsometry (gray bars), on RBS (red bars), and void volume according to VEPALS (blue bars) analysis. Porosity values from ellipsometry are calculated applying the volume averaging theory with an effective medium approximation (see section 2.4), while for RBS it is based on the areal densities (see section 2.3). For void volume equation (1) is applied and averaged over the E_P range from 1 to 3 keV (to ensure only coating contribution).

Table 2. Chemical characterization based on RBS: elemental composition (C, Si, O) and O/Si ratio.

Reactor	DPE or NPC	C (at. %)[a]	Si (at. %)[a]	O (at. %)[a]	O/Si ratio
Symmetric—active	DPE	4.9	27.5	58.4	2.13
electrode	NPC	∼ 0	26.7	57.7	2.16
Asymmetric—grounded	DPE	9.2	28.0	62.8	2.24
electrode	NPC	3.3	30.6	62.6	2.05

[a]Note that the sum of C, Si, and O does add up to 100% for all the samples due to the use of hydrogen in the fitting process. While hydrogen element does not influence the determination of the O/Si ratio, it plays an important role in accurately estimating the total porosity.

secondary ion mass spectrometry characterization [15], with enhanced chemical etching by oxygen species at the surface. In general, the O/Si ratio is always overstoichiometric in oxygen, oscillating between 2.1 and 2.3, unlike a pure silica material.

A labyrinthine pore network with bottlenecks is confirmed by studying the $3\gamma/2\gamma$ ratio from DB-VEPAS (see S6). The obtained results for a very low $3\gamma/2\gamma$ ratio indicate merely a tiny fraction of ortho-Ps detected that we relate to the labyrinthine nanoporous structure of the plasma-deposited layers, representing a worm-like connection of micropores [7]. Similar tendencies and values were observed by Franke *et al* for HMDSO-derived plasma polymer films deposited on PET [11]. These authors relate their $3\gamma/2\gamma$ ratio to an absence of interconnectivity in the nanopore range (component τ_3), therefore calling it a *cluster of vacancies*. In our case, small sub-nanometer-scaled pores around 0.3 nm (component τ_2) are responsible for the transport of small molecules such as water and oxygen, acting as interconnections for larger pores. However, the required size for a free ortho-Ps migration is typically larger, and hence its transport between pores is strongly hindered, considering the ballistic picture only, without even taking into account a larger probability of annihilation due to quenching effects. A clear decrease in $3\gamma/2\gamma$ ratio has also been observed by Zotovich *et al* for UV-treated SiCOH films compared to the pristine material [46]. The short lifetime of ortho-Ps is characteristic of pore walls functionalized by -OH groups due to the high quenching rate (i.e. pick-off annihilation) of hydroxyl groups [47, 48]. Therefore, the larger incorporation of -OH groups during the plasma etching step might also justify the lower $3\gamma/2\gamma$ obtained in our case.

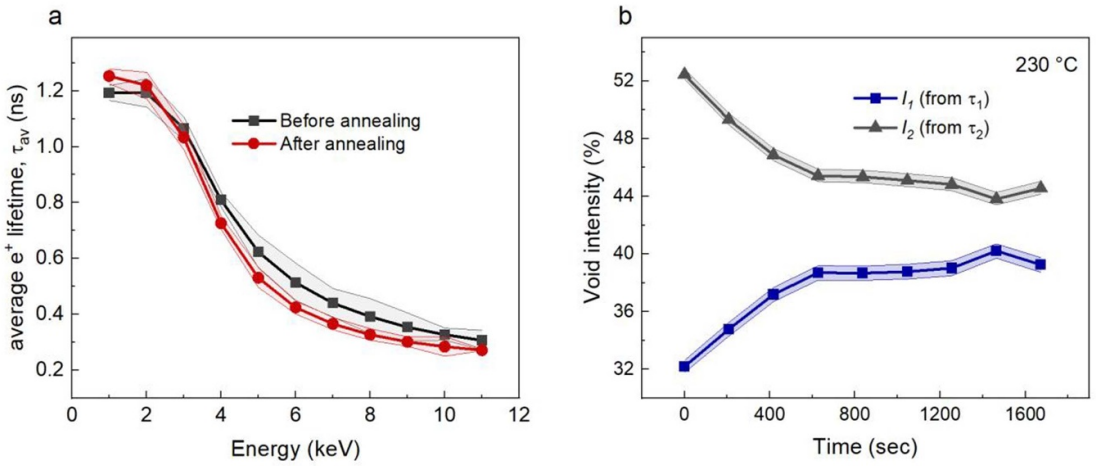

Figure 9. VEPALS characterization of pp-etch-SiOx coatings showing (a) stability before and after annealing at 230 °C, as well as (b) balancing effects during annealing between I_1 (associated to τ_1) and I_2 (associated to τ_2), which can be related to a contraction of the Si–O–Si network ($E_P = 4$kV). Sample deposited by NPC at the grounded electrode in the asymmetric reactor configuration.

3.4. Microporous network stability after annealing

The superhydrophilic nature of nanoporous plasma polymer films fabricated by cycles of plasma polymerization and etching raised the question whether water infused and trapped in the nanopores could affect the characterization discussed in the previous sections. Moreover, the resistance of the plasma coatings to temperature is an important aspect considering the durability of the films for certain applications. Therefore, we selected the coating characterized by the highest porosity—fabricated at the grounded electrode in the asymmetric configuration via NPC—to be heated in vacuum at 230 °C, analyzing the evolution of pore size depth distribution during and after annealing. As can be seen in figure 9(a) for the average positron lifetime, there are no significant differences between the coating before and after annealing, indicating just a smaller contraction of the film after annealing observed as a minor shift to lower implantation energies. This result could be related to a contraction of the Si–O–Si network, therefore increasing the contribution of small defects and para-Ps (τ_1), as indicated by the changes in I_1 (associated to τ_1) in detriment of I_2 (associated to τ_2), as shown in figure 9(b). No changes were observed for the coating in all discrete lifetime components (τ_1 to τ_4), thus not affecting the nanopore size.

The results confirm a robust microporous network for pp-etch-SiOx plasma polymer films during and after exposure to moderate temperatures (230 °C). It also discards a possible water contribution affecting the characterization exposed in previous sections, indicating that water potentially trapped in the coating must have largely disappeared when exposed to the high vacuum in the VEPALS set-up. This agrees with previous findings that infused water in pp-SiOx is rapidly expelled in dry conditions [49]. The obtained findings support a broad window of applications of nanoporous plasma polymer films, *per se* as advanced membranes [50] or as functional layers, for example, to control the diffusion of small molecules, as we have recently demonstrated for as reactive oxygen species in aqueous media [16].

4. Conclusions

This work provides a detailed characterization of the microporosity in plasma polymer films using PAS. Films were synthesized via sequential cycles of plasma HMDSO polymerization and Ar/O_2 etching, forming an interconnected nanoporous network through selective removal of residual hydrocarbons. The resulting coatings exhibit a labyrinthine structure with bottlenecks, consistent with previous molecular dynamics simulations.

Porosity at the sub-nanometer scale was effectively tuned by adjusting reactor design, controlling densification effects attributed to ion bombardment. Compared to dense SiO_2-like barrier layers, the engineered coatings demonstrate significantly enhanced porosity, particularly when applying our recently developed NPC approach. This method enables efficient hydrocarbon removal and, therefore, carbon reduction, directly contributing to increased free volume.

Quantitative analysis via ellipsometry and RBS reveals porosity enhancements up to around 25%, with a void (open) volume reaching 36.8% according to positron lifetime spectroscopy. Lifetime component analysis identifies a dominant population of ∼0.3 nm nanopores within the Si–O–Si cage structure, contributing approximately 60% to the total porosity. Larger nanopores (∼0.65 nm), functionalized with silanol groups, contribute around 25%, while pores in the 0.7–2 nm range account for only 5%. No defects larger than 2 nm were detected, confirming the well-defined coating structure.

The combination of well-defined microporosity and high durability under aqueous, oxidative, and thermal conditions supports a broad range of potential applications. In addition to previously demonstrated uses such as reactive oxygen species delivery and lubrication, these superhydrophilic, glass-like surfaces show promise for emerging applications including adhesion promotion and ultra-thin dielectric layers.

Data availability

All data that support the findings of this study are included within the article (and any supplementary files).

Supplementary data available at http://doi.org/10.1088/1361-6463/ae2c07/data1.

Acknowledgments

This work was supported by SNSF, project COST 2022, n° 213368 (Switzerland), the Initiative and Networking Fund of the Helmholtz Association (FKZ VH-VI-442 Memriox), and the Helmholtz Energy Materials Characterization Platform (03ET7015). Parts of this research have been carried out at Helmholtz-Zentrum Dresden-Rossendorf e. V. (HZDR), Germany, a member of the Helmholtz Association, specifically, at the Ion Beam Center (IBC) and the ELBE Center for High-Power Radiation Sources. The authors thank the HZDR facility staff for their assistance (Ahmed G Attallah). Michał Góra at Empa, St. Gallen, is acknowledged for valuable inputs and discussions.

Conflict of interest

The authors declare no competing financial interest.

Author contributions

Paula Navascués 0000-0002-2762-6527
Conceptualization (lead), Data curation (equal), Formal analysis (equal), Investigation (lead), Methodology (lead), Supervision (equal), Validation (equal), Visualization (equal), Writing – original draft (lead), Writing – review & editing (equal)

Aurelio Garcia-Valenzuela 0000-0002-5238-6465
Formal analysis (equal), Investigation (equal), Methodology (equal), Visualization (equal), Writing – review & editing (equal)

Maciej Oskar Liedke 0000-0001-7933-7295
Formal analysis (equal), Investigation (equal), Methodology (equal), Resources (equal), Writing – review & editing (equal)

Flaela Kalemi 0009-0008-8661-7015
Investigation (equal), Methodology (equal), Validation (equal), Writing – review & editing (equal)

Barbara Hanselmann
Investigation (equal), Validation (equal), Writing – review & editing (equal)

Maik Butterling 0000-0003-3674-0767
Methodology (equal), Software (equal), Writing – review & editing (equal)

Eric Hirschmann 0000-0001-5782-9627
Investigation (equal), Methodology (equal), Software (equal), Writing – review & editing (equal)

Andreas Wagner 0000-0001-7575-3961
Funding acquisition (equal), Project administration (equal), Resources (equal), Writing – review & editing (equal)

Dirk Hegemann 0000-0003-4226-9326
Conceptualization (equal), Funding acquisition (lead), Investigation (lead), Methodology (equal), Project administration (lead), Resources (equal), Supervision (lead), Validation (equal), Writing – review & editing (equal)

References

[1] Shamiryan D, Abell T, Iacopi F and Maex K 2004 Low-*k* dielectric materials *Mater. Today* **7** 34–39
[2] Feng X, Zhu J, Jin J, Wang Y, Zhang Y and Van der Bruggen B 2024 Polymers of intrinsic microporosity for membrane-based precise separations *Prog. Mater. Sci.* **144** 101285
[3] Chen X, Wu L, Yang H, Qin Y, Ma X and Li N 2021 Tailoring the microporosity of polymers of intrinsic microporosity for advanced gas separation by atomic layer deposition *Angew. Chem. Int. Ed.* **60** 17875–80
[4] Coad B R, Favia P, Vasilev K and Griesser H J 2022 Plasma polymerization for biomedical applications: a review *Plasma Process Polym.* **19** 2200121
[5] Fridman A 2023 *Plasma Science and Technology* (Wiley)
[6] Yasuda H 1985 *Plasma Polymerization* (Academic Press)
[7] Attallah A G, Koehler N, Liedke M O, Butterling M, Hirschmann E, Ecke R, Schulz S E and Wagner A 2020 Thermal kinetics of free volume in porous spin-on dielectrics: exploring the network- and pore-properties *Microporous Mesoporous Mater.* **308** 110457
[8] Steele J J and Brett M J 2007 Nanostructure engineering in porous columnar thin films: recent advances *J. Mater. Sci., Mater. Electron.* **18** 367–79
[9] Barranco A, Borras A, Gonzalez-Elipe A R and Palmero A 2016 Perspectives on oblique angle deposition of thin films: from fundamentals to devices *Prog. Mater. Sci.* **76** 59–153
[10] Obrero J M *et al* 2024 Conformal TiO_2 aerogel-like films by plasma deposition: from omniphobic antireflective coatings to perovskite solar cell photoelectrodes *ACS Appl. Mater. Interfaces* **16** 39745–60
[11] Franke J, Zysk F, Wilski S, Liedke M O, Butterling M, Attallah A G, Wagner A, Kühne T D and Dahlmann R 2024 Consideration of the effect of nanoscale porosity on mass transport phenomena in PECVD coatings *J. Appl. Phys.* **57** 405303
[12] Hoppe C, Mitschker F, Butterling M, Liedke M O, de Los Arcos T, Awakowicz P, Wagner A and Grundmeier G 2020 Characterisation of micropores in plasma deposited SiOx films by means of positron annihilation lifetime spectroscopy *J. Phys. D: Appl. Phys.* **53** 475205
[13] Navascués P, Schütz U, Hanselmann B and Hegemann D 2024 Near-plasma chemical surface engineering *Nanomaterials* **14** 195
[14] Gergs T, Monti C, Gaiser S, Amberg M, Schütz U, Mussenbrock T, Trieschmann J, Heuberger M and Hegemann D 2022 Nanoporous SiOx plasma polymer films as carrier for liquid-infused surfaces *Plasma Process Polym.* **19** 2200049
[15] Góra M, Navascués P, Alinezhadfar M, Southam A, Hegemann D and Heuberger M 2025 Hydrophilic nano-porous model surfaces suitable for direct force measurements *Appl. Surf. Sci.* **708** 163776
[16] Navascués P *et al* n.d. Plasma functionalization enables diffusion control of reactive oxygen species *Small* **n/a** 2502311
[17] Gidley D W, Peng H-G and Vallery R S 2006 Positron annihilation as a method to characterize porous materials *Annu. Rev. Mater. Res.* **36** 49–79
[18] Hodges C H and Stott M J 1973 Work functions for positrons in metals *Phys. Rev. B* **7** 73–79
[19] Tao S J 1972 Positronium annihilation in molecular substances *J. Chem. Phys.* **56** 5499–510
[20] Eldrup M, Lightbody D and Sherwood J N 1981 The temperature dependence of positron lifetimes in solid pivalic acid *Chem. Phys.* **63** 51–58
[21] Hoppe C *et al* 2022 Influence of surface activation on the microporosity of PE-CVD and PE-ALD SiOx thin films on PDMS *Plasma Process Polym.* **19** 2100174
[22] Creatore M, Palumbo F, d'Agostino R and Fayet P 2001 RF plasma deposition of SiO_2-like films: plasma phase diagnostics and gas barrier film properties optimisation *Surf. Coat. Technol.* **142–144** 163–8
[23] Grüniger A, Bieder A, Sonnenfeld A, von Rohr P R, Müller U and Hauert R 2006 Influence of film structure and composition on diffusion barrier performance of SiOx thin films deposited by PECVD *Surf. Coat. Technol.* **200** 4564–71
[24] Mitschker F, Wißing J, Hoppe C, de Los Arcos T, Grundmeier G and Awakowicz P 2018 Influence of average ion energy and atomic oxygen flux per Si atom on the formation of silicon oxide permeation barrier coatings on PET *J. Phys. D: Appl. Phys.* **51** 145201
[25] Wagner A, Butterling M, Liedke M O, Potzger K and Krause-Rehberg R 2018 Positron annihilation lifetime and doppler broadening spectroscopy at the ELBE facility *AIP Conf. Proc.* **1970** 040003
[26] Hirschmann E, Butterling M, Hernandez Acosta U, Liedke M O, Attallah A G, Petring P, Görler M, Krause-Rehberg R and Wagner A 2021 A new system for real-time data acquisition and pulse parameterization for digital positron annihilation lifetime spectrometers with high repetition rates *J. Inst.* **16** P08001
[27] Krause-Rehberg R and Leipner H S 1999 *Positron Annihilation in Semiconductors: Defect Studies* (Springer)
[28] Olsen J V, Kirkegaard P, Pedersen N J and Eldrup M 2007 PALSfit: a new program for the evaluation of positron lifetime spectra *Phys. Status Solidi c* **4** 4004–6
[29] Tuomisto F and Makkonen I 2013 Defect identification in semiconductors with positron annihilation: experiment and theory *Rev. Mod. Phys.* **85** 1583–631
[30] Liedke M O *et al* 2015 Open volume defects and magnetic phase transition in Fe60Al40 transition metal aluminide *J. Appl. Phys.* **117** 163908
[31] Anwand W, Brauer G, Butterling M, Kissener H R and Wagner A 2012 Design and construction of a slow positron beam for solid and surface investigations *Defect Differ. Forum* **331** 25–40
[32] Clement M, de Nijs J M M, Balk P, Schut H and van Veen A 1996 Analysis of positron beam data by the combined use of the shape- and wing-parameters *J. Appl. Phys.* **79** 9029–36
[33] Charlton M and Humberston J W 2009 *Positron Physics* (Cambridge University Press)
[34] Coleman P G, Sharma S C and Diana L M 1982 *Positronium Formation in Condensed Matter and High-density Gases* (North-Holland Pub. Co.)
[35] Mayer M 1999 SIMNRA, a simulation program for the analysis of NRA, RBS and ERDA *AIP Conf. Proc.* **475** 541–4
[36] Braun M M and Pilon L 2006 Effective optical properties of non-absorbing nanoporous thin films *Thin Solid Films* **496** 505–14

[37] Hegemann D, Bülbül E, Hanselmann B, Schütz U, Amberg M and Gaiser S 2021 Plasma polymerization of hexamethyldisiloxane: revisited *Plasma Process. Polym.* **18** 2000176
[38] Blanchard N E, Naik V V, Geue T, Kahle O, Hegemann D and Heuberger M 2015 Response of plasma-polymerized hexamethyldisiloxane films to aqueous environments *Langmuir* **31** 12944–53
[39] Wada K and Hyodo T 2013 A simple shape-free model for pore-size estimation with positron annihilation lifetime spectroscopy *J. Phys. Conf. Ser.* **443** 012003
[40] Franke J, Liedke M O, Dahmen P, Butterling M, Attallah A G, Wagner A, Alizadeh P and Dahlmann R, 2024 Influence of coating structure of an SiOx barrier coating on a PET substrate on water vapor permeation activation energy, *Proc. 39th Int. Conf. of the Polymer Processing Society* Ediciones Uniandes (https://doi.org/10.51573/Andes.PPS39.GS.NN.1)
[41] Hegemann D, Körner E, Blanchard N, Drabik M and Guimond S 2012 Densification of functional plasma polymers by momentum transfer during film growth *Appl. Phys. Lett.* **101** 211603
[42] Zhou W, Bailey S, Sooryakumar R, King S, Xu G, Mays E, Ege C and Bielefeld J 2011 Elastic properties of porous low-k dielectric nano-films *J. Appl. Phys.* **110** 043520
[43] Baklanov M R, Mogilnikov K P, Polovinkin V G and Dultsev F N 2000 Determination of pore size distribution in thin films by ellipsometric porosimetry *J. Vac. Sci. Technol. B* **18** 1385–91
[44] García-Valenzuela A *et al* 2020 Positron annihilation analysis of nanopores and growth mechanism of oblique angle evaporated TiO_2 and SiO_2 thin films and multilayers *Microporous Mesoporous Mater.* **295** 109968
[45] Deng S, Kurttepeli M, Cott D J, Bals S and Detavernier C 2015 Porous nanostructured metal oxides synthesized through atomic layer deposition on a carbonaceous template followed by calcination *J. Mater. Chem. A* **3** 2642–9
[46] Zotovich A I *et al* 2022 Modification of porous ultralow-k film by vacuum ultraviolet emission *ACS Appl. Electron. Mater.* **4** 2760–76
[47] He C, Ohdaira T, Oshima N, Muramatsu M, Kinomura A, Suzuki R, Oka T and Kobayashi Y 2007 Evidence for pore surface dependent positronium thermalization in mesoporous silica/hybrid silica films *Phys. Rev. B* **75** 195404
[48] He C, Oka T, Kobayashi Y, Oshima N, Ohdaira T, Kinomura A and Suzuki R 2007 Positronium annihilation and pore surface chemistry in mesoporous silica films *Appl. Phys. Lett.* **91** 024102
[49] Hegemann D, Hocquard N and Heuberger M 2017 Nanoconfined water can orient and cause long-range dipolar interactions with biomolecules *Sci. Rep.* **7** 17852
[50] de Los Arcos T *et al* 2024 PECVD and PEALD on polymer substrates (part II): understanding and tuning of barrier and membrane properties of thin films *Plasma Process Polym.* **21** 2300186